GEOFLUIDS

Geofluids (2010) **10**, 193–205 doi: 10.1111/j.1468-8123.2010.00278.x

Permeability of the continental crust: dynamic variations inferred from seismicity and metamorphism

S. E. INGEBRITSEN[1] AND C. E. MANNING[2]

[1]*US Geological Survey, Menlo Park, CA, USA;* [2]*Department of Earth and Space Sciences, UCLA, Los Angeles, CA, USA*

ABSTRACT

The variation of permeability with depth can be probed indirectly by various means, including hydrologic models that use geothermal data as constraints and the progress of metamorphic reactions driven by fluid flow. Geothermal and metamorphic data combine to indicate that mean permeability (k) of tectonically active continental crust decreases with depth (z) according to $\log k \approx -14$–$3.2 \log z$, where k is in m^2 and z in km. Other independently derived, crustal-scale k–z relations are generally similar to this power-law curve. Yet there is also substantial evidence for local-to-regional-scale, transient, permeability-generation events that entail permeabilities much higher than these mean k–z relations would suggest. Compilation of such data yields a fit to these elevated, transient values of $\log k \approx -11.5$–$3.2 \log z$, suggesting a functional form similar to that of tectonically active crust, but shifted to higher permeability at a given depth. In addition, it seems possible that, in the absence of active prograde metamorphism, permeability in the deeper crust will decay toward values below the mean k–z curves. Several lines of evidence suggest geologically rapid (years to 10^3 years) decay of high-permeability transients toward background values. Crustal-scale k–z curves may reflect a dynamic competition between permeability creation by processes such as fluid sourcing and rock failure, and permeability destruction by processes such as compaction, hydrothermal alteration, and retrograde metamorphism.

Key words: permeability, geothermal, metamorphism, seismicity

Received 14 September 2009; accepted 17 January 2010

Corresponding author: S. E. Ingebritsen, US Geological Survey, Menlo Park, CA 94025, USA.
Email: seingebr@usgs.gov. Tel: 1-650-329-4422. Fax: 1-650-329-4463.

Geofluids (2010) **10**, 193–205

INTRODUCTION

Permeability (k) is a measure of the relative ease of fluid flow under unequal pressure. The permeability of the Earth's crust to aqueous fluids is of great interest because it largely determines the feasibility of important geologic processes such as advective solute transport, advective heat transport, and the generation of elevated fluid pressures by processes such as physical compaction, heating, and mineral dehydration. Yet the measured permeability of the shallow continental crust is so highly variable that it is often considered to defy systematic characterization. The permeability of common geologic media varies by approximately 16 orders of magnitude, from values as low as 10^{-23} m^2 in intact crystalline rock, intact shales, and fault gouge, to values as high as 10^{-7} m^2 in well-sorted gravels. In the upper crust, permeability exhibits extreme heterogeneity, both among geologic units and within particular units. Field-based measurements of layered ash-flow tuff show up to 10^4-fold variation between welded and unwelded zones (e.g. Winograd 1971). Similarly large variations have been measured within single soil units (Mitchell 1993). Even larger variations in *in situ* permeability have been inferred between basalts near the surface of Kilauea volcano ($k \sim 10^{-10}$ to 10^{-9} m^2) and compositionally identical rocks at 1- to 2-km depth ($k \sim 10^{-16}$ to 10^{-15} m^2) (Ingebritsen & Scholl 1993). In many geologic environments, there is also large permeability anisotropy, which is conventionally defined as the ratio between the horizontal and vertical permeabilities but may also reflect variously oriented stratigraphic, structural, and/or tectonic fabrics.

Permeability varies in time as well as space. Temporal variability in permeability is particularly pronounced in hydrothermal environments characterized by strong chemical and thermal disequilibrium. Laboratory experiments involving hydrothermal flow in crystalline rocks under pressure, temperature, and chemistry gradients often result in

© 2010 Blackwell Publishing Ltd

order-of-magnitude permeability decreases over daily to subannual time scales (e.g. Summers *et al.* 1978; Morrow *et al.* 1981, 2001; Moore *et al.* 1983, 1994; Vaughan *et al.* 1986; Tenthorey *et al.* 1998; Cox *et al.* 2001; Zhang *et al.* 2001; Polak *et al.* 2003; Yasuhara *et al.* 2006). Field observations of continuous, cyclic, and episodic hydrothermal-flow transients at various time scales also suggest transient variations in permeability (e.g. Baker *et al.* 1987, 1989; Titley 1990; Hill 1993; Urabe 1995; Haymon 1996; Fornari *et al.* 1998; Sohn *et al.* 1998; Gillis & Roberts 1999; Johnson *et al.* 2000; Golden *et al.* 2003; Husen *et al.* 2004; Sohn 2007). The occurrence of active, long-lived (10^3–10^6 years) hydrothermal systems (Cathles *et al.* 1997), despite the tendency for permeability to decrease with time, implies that other processes such as hydraulic fracturing and earthquakes regularly create new flow paths (e.g. Rojstaczer *et al.* 1995). Indeed there have been suggestions that crustal-scale permeability is a dynamically self-adjusting or even emergent property (e.g. Rojstaczer *et al.* 2008).

This study reviews studies of crustal-scale permeability–depth relations in the last decade. Our earlier work emphasized tectonically active regions of the continental crust and focused on permeability averaged over large time and length scales (Ingebritsen & Manning 1999; Manning & Ingebritsen 1999). Here, we show that independent studies generally agree on values of crustal permeability at such scales. However, we extend these results by surveying recent observations of high permeabilities associated with shorter time and length scales, and by considering permeability decay.

CRUSTAL-SCALE PERMEABILITY–DEPTH RELATIONS

Permeability is heterogeneous, anisotropic, and transient. Nevertheless, some order has been revealed in globally compiled data. In the early 1980s it was proposed, based on compilations of *in situ* hydraulic-test data, that the mean *in situ* permeability of crystalline rocks in the uppermost crust (<1-km depth) is approximately 10^{-14} m^2 (Brace 1980). This result for the very shallow crust is borne out by more recent *in situ* data (Hsieh 1998), whereas other *in situ* data suggest an identifiable decrease in permeability with depth (Clauser 1992).

Direct *in situ* measurements of permeability are rare below depths of 2–3 km and nonexistent below 10-km depth. As an alternative, geothermal data and estimates of fluid flux during prograde metamorphism have been used to constrain the permeability of regions of the continental crust undergoing active metamorphism and tectonism. A power-law fit to these data yields

$$\log k \approx -14 - 3.2 \log z, \tag{1}$$

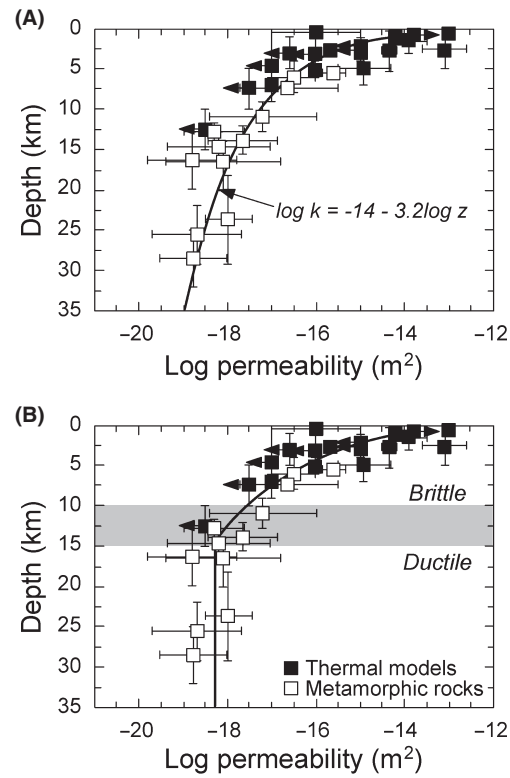

Fig. 1. Estimates of permeability based on hydrothermal modeling and the progress of metamorphic reactions showing (A) power-law fit to data and (B) data below 12.5-km depth fitted with a constant value of $10^{-18.3}$ m^2 (after Manning & Ingebritsen 1999; Ingebritsen & Manning 2002).

where k is in m^2 and z is in km (Manning & Ingebritsen 1999). This empirical fit (Fig. 1A) defines a value of log k at 1-km depth (−14) that is equivalent to Brace's (1980) mean *in situ* permeability of crystalline rocks. Assuming the depth of the brittle–ductile transition in tectonically active crust to be 10–15 km and fitting the data in each regime separately (Fig. 1B) implies effectively constant permeability of $\log k \approx -18.3$ below 15 km. Townend & Zoback (2000) found eqn 1 to be compatible with data from *in situ* hydraulic tests and from seismicity induced either by fluid injection or reservoir impoundment.

The 'geothermal–metamorphic' permeability–depth relation (eqn 1, Fig. 1) has since been used successfully in modeling crustal-scale fluid flow (Lyubetskaya & Ague 2009) and been shown to be reasonably compatible with other independently compiled data (Shmonov *et al.* 2002, 2003; Saar & Manga 2004; Stober & Bucher 2007). Field permeability measurements (35 soil samples) and lab experiments at high pressure and temperature (11 samples, 237 experimental points to 600°C, 200 MPa) by Shmonov *et al.* (2003) yield a similar relation,

$$\log k \approx -12.56 - 3.225 z^{0.223} \tag{2}$$

with k and z again in m^2 and km, respectively. In this case, $-\log k$ at 1-km depth is 15.6. Saar & Manga (2004)

developed a model for the permeability structure of the central Oregon Cascades based on several lines of evidence, including springflow characteristics, matching of geothermal data, hydrologically induced seismicity at Mount Hood, and the permeability needed for escape of magmatic volatiles at depth. Their results agreed with the geothermal–metamorphic curve (eqn 1) except at relatively shallow depths (≤0.8 km), where they proposed instead

$$k \approx 5 \times 10^{-13}\mathrm{m}^2 \exp\left(\frac{-z}{25\,\mathrm{km}}\right), \tag{3}$$

which fits their shallow data better and allows for a finite near-surface permeability. In this case, $-\log k$ at 1-km depth is approximately 15. Most recently, an empirical fit to *in situ* data from ≤4.5-km depth in the Black Forest, Germany, yielded

$$\log k \approx -15.4 - 1.38 \log z \tag{4}$$

with k and z again in m^2 and km, respectively (Stober & Bucher 2007).

Figure 2 compares these three proposed crustal-scale permeability–depth relations (eqns 1, 2, and 4), all of which implicitly assume permeability to be isotropic. The permeability trend based on original experimental data (eqn 2) can be viewed as representing the crust under isotropic stress conditions in a state of mechanical and chemical equilibrium (Shmonov *et al.* 2003). The geothermal–metamorphic curve (Fig. 1A, eqn 1) represents natural systems averaged over large spatial scales and long time scales. Individual metamorphic-permeability values are based on time-integrated fluid flux over the (generally long) time span of a metamorphic event. They are obtained by solving a one-dimensional form of Darcy's law suitable for variable-density fluids,

$$q_x = \left(\frac{\bar{k}}{\mu}\right)\left(-\frac{\partial(P + \rho g z)}{\partial x}\right), \tag{5}$$

for time-averaged permeability $\bar{k}$,

$$\bar{k} = \left(\frac{Q\mu}{\Delta t(\partial[P + \rho g z]/\partial x)}\right), \tag{6}$$

where q_x is the volumetric fluid flow along the flow path x, ρ is fluid density, g is gravitational acceleration, z is elevation above a datum, μ is the dynamic viscosity of the fluid, $(\partial[P + \rho g z]/\partial x)$ is the energy gradient for flow along x, Q is the time-integrated fluid flux, and Δt is the duration of metamorphism, so that $q_x = Q/\Delta t$. The time-integrated fluid flux Q is a key parameter in many metamorphic studies. It is calculated on the basis of fluid-driven changes in rock composition and mineral assemblages.

The metamorphic permeabilities (Figs. 1 and 2) represent environments in which fluid flow was or is a consequence of tectonic or magmatic activity. It has been suggested that lower permeabilities might be expected during metamorphism associated with cooling and decompression (cf. Yardley & Baumgartner 2007), or in the deep crust in stable cratons (cf. Ingebritsen & Manning 2002). This suggestion is consistent with the fact that mean geothermal–metamorphic permeabilities (eqn 1) are roughly one order of magnitude larger than mean 'experimental' permeabilities (eqn 2) (see Fig. 2). The 'Black Forest' permeability curve, which represents a tectonically active rifting environment and is empirically constrained only at shallow (<5 km) depths, lies between the experimental and geothermal–metamorphic curves (Fig. 2).

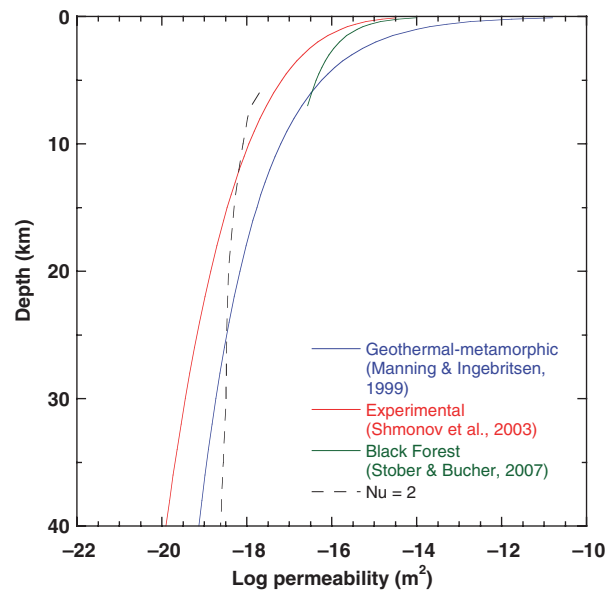

Fig. 2. Crustal-scale permeability–depth curves based on geothermal–metamorphic (Manning & Ingebritsen 1999), experimental (Shmonov *et al.* 2003), and Black Forest (Stober & Bucher 2007) data. The permeability associated with advection-dominated heat transport (Nu > 2) in the lower crust is calculated assuming a driving-force gradient of 10 MPa km^{-1}, a temperature gradient of 25°C km^{-1}, and a thermal conductivity of 2 W $(\mathrm{m\,K})^{-1}$, and ranges from $\log k \sim -18.1\ \mathrm{m}^2$ at 10-km depth to $\log k \sim -18.6\ \mathrm{m}^2$ at 40-km depth. The permeability associated with Nu 2 in the upper crust (0- to 10-km depth) will typically be about 2 orders of magnitude higher ($\log k \sim -16\ \mathrm{m}^2$) because of the lower fluid viscosities and much lower driving-force gradients for fluid flow. The permeability associated with a Sherwood number Sh ~ 2 in the deeper crust would be approximately 10^4 times lower than that associated with Nu ~ 2 (as per Bickle & McKenzie 1987, their fig. 6); that is, $\log k \sim -22\ \mathrm{m}^2$.

EVIDENCE FOR HIGHER PERMEABILITIES

The permeability–depth relations portrayed in Figure 2 are reasonably consistent. However, on short time scales, permeability may reach values significantly in excess of those represented by eqns 1, 2, and 4. There is now a growing body of evidence that allows examination of whether there are systematic variations in this behavior with depth. The evidence includes rapid migration of seismic hypocenters, enhanced rates of metamorphic reaction

in major fault or shear zones, and recent studies suggesting much more rapid metamorphism than has been canonically assumed (Table 1).

Space–time progression of earthquake fronts

Certain well-located earthquake swarms exhibit space–time progression of seismicity fronts that develop roughly as the square root of time, consistent with earthquake triggering by diffusive propagation of an aqueous-fluid pressure front (Fig. 3). Rates of hypocenter migration can be used to calculate a range of hydraulic diffusivities D according to

$$r = (4\pi Dt)^{1/2}, \tag{7}$$

where r is the distance and t is the time (Talwani & Acree 1984; Shapiro *et al.* 1997). Hydraulic diffusivity is related to hydraulic conductivity K through

$$K = DS_s, \tag{8}$$

where

$$S_s = \rho g(\alpha + n\beta), \tag{9}$$

ρ is the density of the aqueous phase, g is the gravitational acceleration, α is the bulk compressibility of the medium, n is porosity, and β is the compressibility of the aqueous phase. Permeability k can then be calculated from hydraulic conductivity via

Table 1 Evidence for relatively high crustal-scale permeabilities.

Locality	Depth (km)	Diffusivity ($m^2\ s^{-1}$)	Log k (m^2)	Reference
Migration of seismic hypocenters				
Matsuhiro 1965–1967 (V)	0–6		−12.6	Cappa *et al.* (2009)
Remiremont 1984 (H)	6–8		−16 to −13	Audin *et al.* (2002)
Yellowstone 1985 (H)	2.5–9	10	−12.7	Waite & Smith (2002)
Mammoth Mtn. 1989 (V)	2–6	0.2–0.6	−14.4 to −13.9	Hill & Prejean (2005)
Mammoth Mtn. 1989 (H)	5–6	0.03–0.06	−15.2 to −14.9	Hill & Prejean (2005)
Dobi (Afar) 1989 (H)	5.5–11.6		−8.3 to −7.3	Noir *et al.* (1997)
Antofagasta 1995 (V)	34–38		−13.3	Nippress & Rietbrock (2007)
South Moat, Long Valley 1997 (H)	4–9	12–90	−12.7 to −11.8	D.P. Hill, USGS, written communication
Umbria-Marche 1997	1–8		−10.4	Miller *et al.* (2004)
West Bohemia 2000	7–10	0.27	−14.4	Horalek & Fischer (2008)

Locality	Depth	Log k	Reference
Fault-zone metamorphism			
Hunts Brook, CT	22.3 ± 3.7*	−15.8	Dipple & Ferry (1992)
Finero, Italy	22.3 ± 3.7*	−16.3	Dipple & Ferry (1992)
Storo, Greenland	22.3 ± 3.7*	−15.8	Dipple & Ferry (1992)
Grimsel, Switzerland	14.9 ± 3.7*	−16.45	Dipple & Ferry (1992)
Broken Hill, Aust.	14.9 ± 3.7*	−16.15	Dipple & Ferry (1992)
Aar Massif, Switz.	9.7–13.4	−17.1 to −15.1	Challandes *et al.* (2008)

Locality	Depth	Δt (previous Δt)	Log k	Reference
Temporally focused heating				
Scotland (regional)	12–15.6	0.3 (3 Ma)	−17.4 to −15.6	Ague & Baxter (2007)
Connecticut (reg.)	18.2–29.2	2 (13 Ma)	−17.7 to −16.7	Lancaster *et al.* (2008)

Locality	Depth	Log k	Reference
Anthropogenic seismicity			
Rocky Mtn. Arsenal, CO	3.7–7.0	−16.2	Hsieh & Bredehoeft (1981)
KTB, Germany	7.5–9	−16.6 to −16	Shapiro *et al.* (1997)
Soultz, France	2.85–3.4	−14.5†	Evans *et al.* (2005)
Basel, Switzerland	4.6–5.0	−14.4‡	Häring *et al.* (2008)
"Seismogenic k"	0–10	−15.3 to −13.3	Talwani *et al.* (2007)

The designations (V) and (H) for seismic hypocenters indicate dominantly vertical and horizontal migration of the seismicity fronts, respectively. The (previous Δt) noted for temporally focused heating refers to the duration of metamorphism assumed by Manning & Ingebritsen (1999 , their table 2).
*Dipple & Ferry (1992) do not specify uncertainties; our assumed value is the uncertainly commonly quoted for thermobarometry from metamorphic mineral assemblages
†Initial (prestimulation) permeability was log $k \approx -16.8$ (Evans *et al.* 2005).
‡Initial (prestimulation) permeability was log $k \approx -17$ (Häring *et al.* 2008).

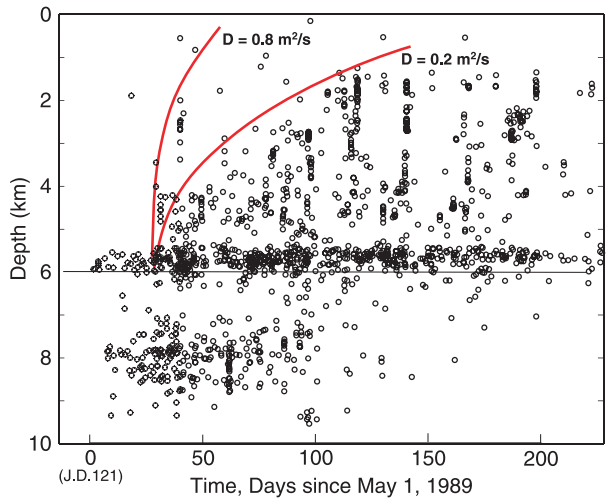

Fig. 3. Seismicity propagation rates provide a constraint on (dynamic) hydraulic diffusivity ($D = r^2/4\pi t$). In the case of the 1989 earthquake swarm beneath Mammoth Mountain, California, $D \sim 0.2$–0.8 m^2 s^{-1} (from Hill & Prejean 2005).

$$k = \mu K/\rho g, \tag{10}$$

where μ is dynamic viscocity and g is the gravitational acceleration. The conversion from D to k introduces substantial uncertainty that owes mainly to the uncertainties associated with ρ, α, n, β, and μ. Table 1 lists k values computed by other authors when available (cf. Miller *et al.* 2004, p. 727). Otherwise, we have converted the reported D values to k by assuming $S_s \approx 10^{-6}$ m^{-1}, following Saar & Manga (2004, p. 11), and calculating ρ and μ for pure water at the mean seismogenic depth assuming a geothermal gradient of 25°C km^{-1}, a mean surface temperature of 10°C, and a hydrostatic pressure gradient.

The examples of hypocenter migration listed in Table 1 yield values of log k ranging from −16 to −7.3, or 1 to 9 orders of magnitude higher than those indicated by the geothermal–metamorphic curve at comparable depths (Fig. 4). The extreme values of log k (−8.3 to −7.3) are for the Dobi earthquake swarm, central Afar. The Dobi seismic sequence traversed fissured basalts. Although such basalts are the most permeable rocks widely exposed at the Earth's surface, the permeability of young, unaltered basalt flows is typically somewhat smaller, with mean log k constrained to be in the range of −11 to −9 in diverse geologic settings [the flanks of the mid-ocean ridge (Stein & Fisher 2003), oceanic islands (Ingebritsen & Scholl 1993), and continental volcanic arcs (Manga 1996, 1997)]. The other examples of hypocenter migration yield log k of −16 to −10.4, well within the range observed in various geologic media near the Earth's surface but unusually high for the given crustal depths.

Fault-zone metamorphism

Our previous compilation of metamorphic-permeability data (Manning & Ingebritsen 1999, their table 2) intentionally omitted major faults and shear zones, as their restricted areal extent and concentration of strain by definition made them anomalous with respect to average properties of the crust. Work on metamorphic data from deep fault zones (Dipple & Ferry 1992, their fig. 4) had already established that fault-zone permeabilities tend to be substantially higher, a finding corroborated by more recent work (Challandes *et al.* 2008). The six examples of fault-zone metamorphism listed in Table 1 yield a mean – and apparently depth-independent (Fig. 4) – permeability of log $k \sim -16.1$. This is 2 orders of magnitude higher than the depth-independent permeability suggested by the metamorphic data set that excludes fault zones (log $k \sim -18.3$, Fig. 1B).

Temporally focused heating

Calculated values of metamorphic permeability are inversely proportional to the duration of metamorphism (Δt in eqn 6). Two recent analyses of metamorphism (Table 1) provide evidence for much more rapid heating than previously assumed, revising the time scale of regional metamorphism from approximately 3 Ma (Ague 1997) to approximately 0.3 Ma in Scotland (Ague & Baxter 2007) and from approximately 13 Ma (Ague 1994) to approximately 2 Ma in Connecticut (Lancaster *et al.* 2008). These revised time scales increase the calculated permeabilities by roughly an order of magnitude, placing permeability during both events well above the mean geothermal–metamorphic permeability–depth curve (Fig. 4). The recalculated permeabilities are large enough to permit significant heat advection (Fig. 2), consistent with the fact that advectively perturbed geotherms have been inferred in each instance (Ague & Baxter 2007; Lancaster *et al.* 2008).

Anthropogenically enhanced permeability

Earthquake triggering by diffusive propagation of an aqueous-fluid pressure front can be initiated by sudden communication between a relatively high-pressure source and lower-pressure surroundings (e.g. Miller *et al.* 2004; Hill & Prejean 2005). This suggests analogy with anthropogenic earthquake triggering via fluid injection (e.g. Fischer *et al.* 2008; Shapiro & Dinske 2009) and reservoir filling (Talwani *et al.* 2007). Studies of waste injection at the Rocky Mountain Arsenal (RMA) (Hsieh & Bredehoeft 1981), the German Continental Deep Drilling Borehole (KTB), and the Soultz and Basel Enhanced Geothermal System (EGS) sites have yielded particularly well-constrained hydraulic parameters. Preinjection permeabilities at

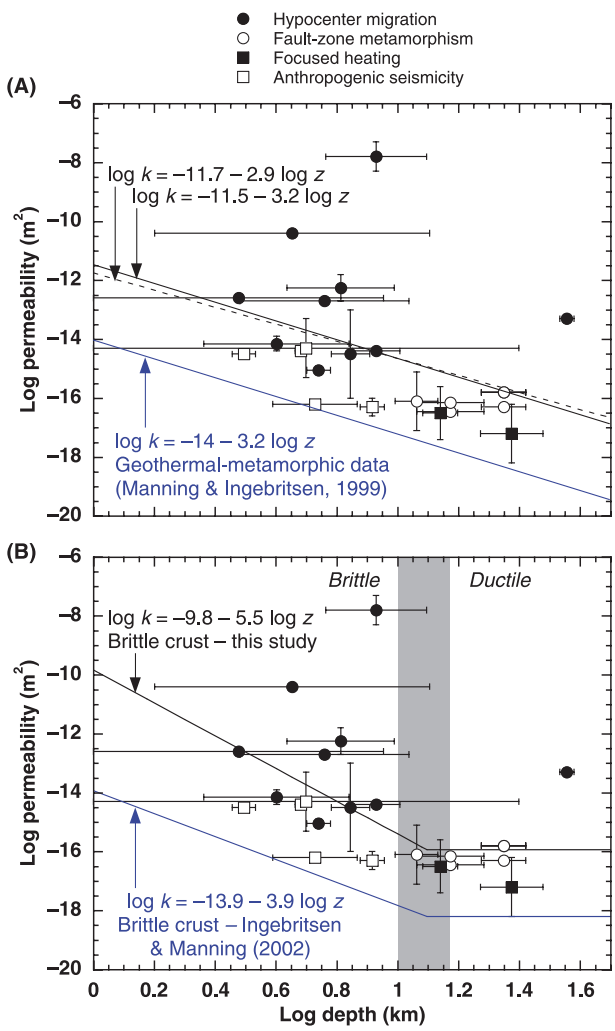

Fig. 4. Evidence for relatively high crustal-scale permeabilities showing (A) power-law fit to data and (B) data below 12.5-km depth fitted with a constant value. Lower curve in both (A) and (B) is the best fit to geothermal–metamorphic data (Fig. 1). Data points are midpoints in reported ranges in k and z for a given locality (Table 1); error bars depict the full permissible range for a plotted locality and are not Gaussian errors.

the RMA are not well known, so comparison of pre- and poststimulation permeabilities is not possible. Fluid-injection-induced hydraulic fracturing at KTB yielded permeabilities near the upper limits of those determined by previous hydraulic testing (Shapiro *et al.* 1997). Fluid injection at 2.85- to 3.45-km depth at Soultz and 4.6- to 5.0-km depth at Basel increased permeability 10^2-fold relative to prestimulation conditions (Evans *et al.* 2005; Häring *et al.* 2008). Finally, a global synthesis of 90 case histories of injection- or reservoir-induced seismicity (Talwani *et al.* 2007) revealed that each episode seems to be associated with permeabilities in the range of log k = −15.3 to −13.3, above the mean range of crustal permeability at comparable depths. These examples of what we collectively term 'anthropogenic seismicity' (Table 1) are 0–2 orders of magnitude higher than those indicated by the geothermal–metamorphic curve (Fig. 4).

PERMEABILITY DECAY AND LOWER BOUNDS

The high permeabilities depicted in Fig. 4 (and Table 1) must be localized and transient. If this were not the case, crustal heat transport would be advection-dominated, and crustal temperatures would be generally lower than they are observed or inferred to be. Large-scale crustal permeabilities greater than the approximate threshold for advective heat transport (approximately 10^{-16} m^2 and 10^{-18} m^2 in the upper and lower crust, respectively) must be relatively rare. Further, the high permeabilities depicted in Fig. 4 would preclude the elevated fluid pressures that are believed to be pervasive below the brittle–ductile transition; overpressures typically require large regions of a flow domain (L > 100 m) to be composed of, or bounded by, material with $k \leq 10^{-17}$ m^2 (Neuzil 1995; Manning & Ingebritsen 1999).

Rates of permeability decay

In the absence of active fluid sourcing and tectonism, permeability should tend to decrease due to processes such as mineral precipitation, hydrothermal alteration, and compaction; however, the rate of this decrease is poorly known. Here we examine various constraints on the rates of permeability decay.

In the introduction, we cited laboratory experiments involving hydrothermal flow in crystalline rocks that result in order-of-magnitude permeability decreases over subannual time scales. Although many laboratory studies involve strong chemical disequilibrium that may not be representative of most natural systems, there are field observations of hydrothermal-flow transients over comparably short time scales. Further, permeability in hydrothermal upflow zones can be drastically reduced by silica precipitation (Lowell *et al.* 1993) or thermoelastic stresses (Germanovich & Lowell 1992) over approximately 10^1 years. Hence, we infer that permeability decay can be very rapid under conditions of strong chemical or thermal disequilibrium.

In situ measurements of permeability decay (Table 2) are particularly relevant, albeit scarce and limited to the brittle upper crust. Some such data owe to observations following co-seismic permeability increases caused by strong ground motion. At the Piñon Flat observatory in the California Coast Ranges, the response of water levels in two shallow (<250 m) wells to solid-Earth tides was used to measure permeability over a 20-year period. Elkhoury *et al.* (2006) found that permeability increased by as much as a factor of 3–4 coincident with seven regional earthquakes, with the magnitude of increase proportional to the peak ground velocity at the site. Between earthquakes,

Table 2 Evidence for changes in *in situ* permeability in the brittle upper crust.

Locality	Depth (km)	k_2/k_1 (m^2)	Reference
Co-seismic permeability increases			
Pinyon Flat 1988–2006	0–0.2	≤4	Elkhoury *et al.* (2006)
Loma Prieta 1989 (H)	Shallow*	~10	Rojstaczer *et al.* (1995)
Kobe 1995 (H)	Shallow*	3–15	Sato *et al.* (2000)
Alum Rock 2007 (V)	Shallow*	3–10	Manga & Rowland (2009)

Locality	Depth (km)	Log k_1 (m^2)	Log k_2 (m^2)	Δt (years)	Reference
Postseismic permeability decreases					
Matsushiro 1965–1970†	0–6	−12.6	−14 to −13	3–5	Ohtake (1974), Cappa *et al.* (2009)
Pinyon Flat 1988–2006	0–0.2	−14.5	−15	2	Elkhoury *et al.* (2006)
Nojima‡ 1997–2003	1.8	−14.4	−15	6	Kitagawa *et al.* (2007)

Locality	Depth (km)	Log k_1 (m^2)	Log k_2 (m^2)	Δt§	Reference
Permeability increases from enhanced geothermal system stimulation					
Soultz, France	2.85–3.4	−16.8	−14.5	15 d	Evans *et al.* (2005)
Basel, Switzerland	4.6–5.0	−17	−14.4	6 d	Häring *et al.* (2008)

For co-seismic permeability increases, V and H denote models inferring dominantly vertical and horizontal fluid flow, respectively.
*Models for the Loma Prieta and Kobe responses are based on lateral groundwater flow in systems with total water-table relief of <1 km. The Alum Rock response entailed minor changes in temperature (1–2°C), suggesting relatively shallow fluid sourcing.
†Co-seismic permeability (1965–1967) based on numerical modeling constrained by ground-deformation data (Cappa *et al.* 2009); postseismic (1970) permeability based on deep-well injection testing (Ohtake 1974).
‡Based on a series of three injection experiments following the 1995 Kobe earthquake.
§Duration of hydraulic stimulation.

permeability decayed steadily toward background values of log $k \sim -15$ m^2 (for one of the two monitored wells) and log $k \sim -14.2$ m^2 (for the other well) over a period of several years (Fig. 5). Numerous investigators have studied the postseismic evolution of permeability in the Nojima, Japan, fault zone following the 1995 Kobe earthquake. Several direct and indirect experiments at Nojima agree that permeability decreased by 40–70% over the 8 years following the earthquake (Tanaka *et al.* 2007).

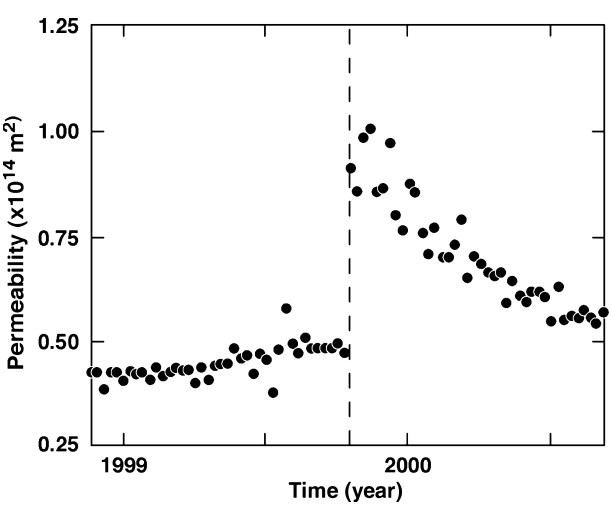

Fig. 5. Permeability response to the 1999 Hector Mine earthquake at the Piñon Flat Observatory, California Coast Ranges (from Elkhoury *et al.* 2010).

Both the California Coast Range study and the Nojima studies entailed direct measurement of permeability. Lillemor Claesson and colleagues have inferred postearthquake permeability decay indirectly on the basis of geochemical changes in wells in northern Iceland (Claesson *et al.* 2007) and northeastern India (Claesson 2007). They inferred substantial permeability decreases over similar time scales of 10^0 to 10^1 years.

Co-seismic changes in streamflow and groundwater levels in the California Coast Ranges also provide inferential evidence for rates of permeability decay. Prior to the 1989 Loma Prieta earthquake, the water table below ridgelines in the Santa Cruz Mountains was very near the land surface, where it could be tapped by shallow wells. The Loma Prieta earthquake caused a roughly 10-fold increase in shallow permeability, resulting in both temporarily increased streamflow and groundwater-level declines that caused shallow wells to go dry (Rojstaczer & Wolf 1994; Rojstaczer *et al.* 1995). On the basis of pre-Loma Prieta conditions, one can reasonably infer that water levels (and permeability) on the San Francisco peninsula had reequilibrated between the time of the great 1906 San Francisco earthquake and the 1989 Loma Prieta earthquake. Further, anecdotal reports indicate partial recovery of water levels between 1989 and the time of this writing (S.A.

Rojstaczer, oral communication, 2009). Thus, we can estimate that decay of a roughly 10-fold increase in shallow permeability in the Coast Ranges requires 10^1 to 10^2 years.

One can also make an inferential argument for rates of fracture healing along the margin of the Skaergaard intrusion, East Greenland, a contact-metamorphic locality where a layered gabbroic intrusion was emplaced at a depth of approximately 3.5 km within a 6- to 7-km-thick section of extrusive basalts. Despite field evidence for multiple episodes of porosity generation and fracturing within about 250 m of the intrusion (Manning & Bird 1991), any associated permeability increase must have been short-lived (approximately $<10^3$ years), because the observed metamorphic mineral assemblages require the high temperatures associated with conduction-dominated cooling (Manning *et al.* 1993).

Initial *ad hoc* attempts to model crustal-scale permeability as a dynamically self-adjusting parameter – conditioned on similar evidence – have assumed that substantial loss of permeability requires times of decades to centuries (Rojstaczer *et al.* 2008). We infer that in dynamic geologic environments, permeability can decay substantially (by a factor of 2–10 or more) over geologically short time scales of 10^0 to 10^3 years.

Table 2 assembles quantitative evidence for magnitudes and rates of *in situ* permeability increase and decrease in the brittle upper crust. Co-seismic shaking associated with regional earthquakes has been observed to cause 3- to 10-fold, quasi-instantaneous increases in the permeability of the uppermost crust. Postseismic permeability decreases of similar magnitude have been observed over periods of several years. The relatively strong hydraulic forcing associated with EGS operations has caused 10^2-fold permeability increases over stimulation periods of days to weeks.

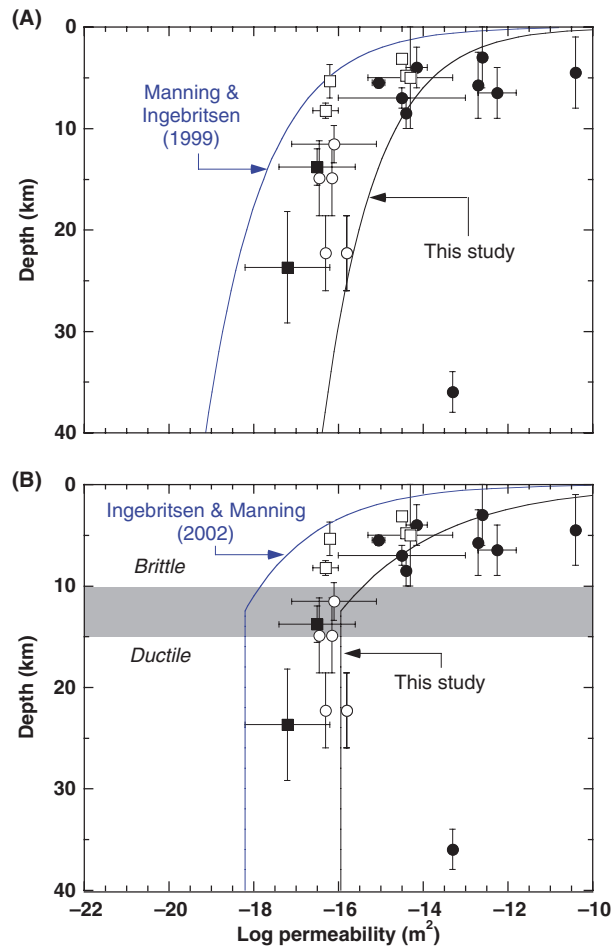

Fig. 6. Evidence for relatively high crustal-scale permeabilities showing (A) power-law fit to data and (B) data below 12.5-km depth fitted with a constant value. Upper curve in both (A) and (B) is the best fit to geothermal–metamorphic data (Fig. 1). 'High-permeability' data points are midpoints in reported ranges in k and z for a given locality (Table 1); error bars depict the full permissible range for a plotted locality and are not Gaussian errors. The Dobi (Afar) earthquake swarm (Table 1) is not shown on this plot (it is off-scale).

Lower limits of crustal permeability?

We have inferred that permeability may decay fairly rapidly from the 'high' values listed in Table 1 and depicted in Figs. 4 and 6. How far will it decay? Is there an identifiable lower bound to crustal permeability?

Conduction-dominated heat transport seems to be the norm below a few kilometers depth in the crust. The importance of heat advection relative to heat conduction can be represented by the Nusselt number Nu, which is the ratio, in a particular dimension, of the total heat transfer to the heat transfer that would be expected in the absence of advection. For conditions in the deeper crust during prograde metamorphism, we can assume dominantly upward flow of both heat and matter and write

$$\mathrm{Nu} = \frac{c_f \rho q_z T + (K_m(T_L - T_U)/L)}{(K_m(T_L - T_U)/L)}, \qquad (11)$$

where c_f, ρ, and T are the heat capacity, density, and temperature of fluid flowing upward at a volumetric rate ($m^3\ m^{-2}$) of q_z, respectively; K_m is the thermal conductivity of the medium; and T_L and T_U are the temperatures at the upper and lower boundaries of a depth interval L, respectively.

Figure 2 shows the approximate lower-crust permeability associated with a Nusselt number of 2 (the level at which advection = conduction) relative to various permeability data. The Nu $\sim$ 2 curve for the lower crust is quite similar to the geothermal–metamorphic and experimental permeability–depth curves. However, all of the high-permeability values of Table 1 would plot well above the Nu $\sim$ 2 curve, and thus seem unlikely to represent long-term stable conditions. Devolatilization-induced metamorphic permeability may be regulated by the heat flow-dependent kinetics of devolatilization. The positive feedback loop depicted in

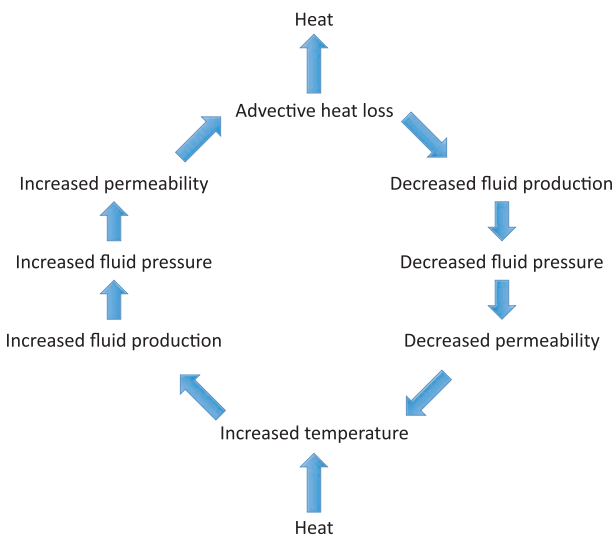

Fig. 7. Feedback between permeability creation and decay during metamorphism. This feedback loop is driven by the heat flow-dependent kinetics of metamorphic devolatilization.

Fig. 7 would tend to constrain long-term average permeability to levels below those at which heat advection becomes significant; that is, Nu $\sim \leq 2$. Thus, we suggest that permeabilities in excess of Nu ~ 2 would decay, perhaps relatively rapidly.

It is difficult to define the lower limit toward which permeability may eventually decay, although the permeability of rocks undergoing retrograde (water-absorbing) metamorphism may be effectively zero (cf. Yardley & Valley 1997; Yardley & Baumgartner 2007). In water-saturated media, the concept of a 'hydrodynamic' permeability governed by Darcy's law (eqn 5) would seem to be less relevant where transport of both heat and solutes is dominantly by diffusion. Because the diffusivity of heat in geologic media is many orders of magnitude greater than diffusivity of any atomic species, there is a large range of permeability within which heat will be largely conducted but solutes largely advected (Bickle & McKenzie 1987). However, below a Sherwood number (mass transfer Nusselt number) of Sh ~ 2, transport of both heat and solutes will be mainly by diffusion. In low-porosity geologic media (0.1% porosity), the permeability associated with Sh ~ 2 will be about 10^4 times lower (Bickle & McKenzie 1987, their fig. 6) than the permeability associated with Nu ~ 2. Most of the permeability data that we have compiled lie well above the permeability associated with Sh ~ 2. This is necessarily the case because all of the metamorphic data points (Fig. 1), for instance, entail positive geochemical evidence for fluid flow.

Even where transport of heat and solutes are largely diffusive, it is possible that hydrodynamic permeability influences fluid pressures, and therefore crustal rheology. In fact, very low permeabilities (cf. $\log k = -24.3$ to -21.3; Audet *et al.* 2009) have been invoked to explain hydrodynamic phenomena. In a water-saturated medium, the concept of hydrodynamic permeability would seem entirely irrelevant only when and where the transport of oxygen (presumably as molecular water) by grain-boundary diffusion (e.g. Farver & Yund 1995) becomes more effective than Darcian flow.

DISCUSSION

Some economic geologists, geophysicists, and metamorphic petrologists have long recognized permeability as a dynamic parameter that changes in response to dewatering and fluid production (e.g. Sibson *et al.* 1975; Walder & Nur 1984; Yardley 1986; Titley 1990; Hanson 1992, 1995, 1997; Dutrow & Norton 1995; Connolly 1997; Cox 2002; Sibson & Rowland 2003; Yardley & Baumgartner 2007). This view is in stark contrast to the hydrogeologic concept of permeability as a static material property that exerts control on fluid flow. The petrologic view of crustal permeability is consistent with indications that fluid pressure is close to the lithostatic load during prograde metamorphism (e.g. Fyfe *et al.* 1978); sufficiently overpressured fluids cannot be contained in the crust and create the permeability necessary to escape. Recently, it has been suggested that the permeability of the brittle upper crust may also be dynamically self-adjusting, responding to tectonism and external fluid sources as much as the lower crust responds to the magnitude of internal fluid sources (cf. Rojstaczer *et al.* 2008). The high-permeability data compiled here (Table 1, Figs 4 and 6) seems compatible with the concept of 'dynamic permeability' (Cathles & Adams 2005).

Like the original compilation of geothermal–metamorphic permeabilities (Fig. 1), the high-permeability data of Table 1 suggest systematic variation with depth (Figs 4 and 6). A quantitative best fit to the data set as a whole yields

$$\log k \approx -11.7 - 2.9 \log z, \tag{12}$$

with k in m^2 and z in km. Fixing the slope at -3.2, the value derived by Manning & Ingebritsen (1999) for 'geothermal–metamorphic' data yields

$$\log k \approx -11.5 - 3.2 \log z, \tag{13}$$

a closely similar result (Fig. 4). These fits are obtained by grouping all of the 'high-permeability' data of Table 1. Considered separately, the data from below 12.5 km appear depth-independent, like the geothermal–metamorphic data.

The apparently similar organization of the geothermal–metamorphic and grouped 'high-permeability' data prompts consideration of the physical implications of the

empirical constants in the curve fits. The constant −14 of the original power-law geothermal–metamorphic curve (the permeability at 1-km depth from eqn 1) is similar to the mean permeability of the uppermost crust, as defined independently both by *in situ* well-test data (Brace 1980) and recharge-based calculations (Rojstaczer *et al.* 2008). The coefficient −3.2 can be inferred to reflect the magnitude of deep metamorphic (or other endogeneous) fluid fluxes. The similar form of the geothermal–metamorphic and high-permeability curves (eqns 1, 12, and 13) may perhaps reflect a confining-pressure dependence of porosity–strain and permeability–strain relations (cf. Cox *et al.* 2001, his fig. 1).

Both the original geothermal–metamorphic data set (Fig. 1) and the 'high-permeability' data set (Figs 4 and 6) suggest a high variance and strong depth dependence of permeability at crustal depths of about <10 km, with less variance and essentially no depth dependence below 10-km depth. This supports a general distinction between the hydrodynamics of a brittle upper crust and a ductile lower crust that is dominated by devolatilization reactions and internally derived fluids. Both data sets can reasonably be fitted with a constant value of log k below 10-km depth, again with an offset of about 2 orders of magnitude (log $k \sim -18.3$ versus log $k \sim -16.0$).

In the deeper crust, the rough coincidence of the geothermal–metamorphic curve and the curve for $\mathrm{Nu} \sim 2$ (Fig. 2) lends credence to the concept of thermally self-regulating metamorphic permeability (Fig. 7), as does the brevity of the episodes of heat advection inferred for metamorphism in Connecticut and Scotland (Table 1; Ague & Baxter 2007; Lancaster *et al.* 2008). Although the 'high-permeability' values summarized in Table 1 may be ephemeral in the context of geologic time, they can be crucially important from the standpoint of heat and mass transport. However, even these 'high-permeability' values for metamorphism are probably not the true transient permeabilities. In prograde metamorphism, fluid generation is an intermittent process that switches on an off when reaction boundaries are crossed. Produced fluid migrates through the crust as a high porosity/permeability wave (Connolly 1997). All of the common petrologic methods yield a time-integrated fluid flux and an average permeability, so that the full cycles of permeability build-up and decay are extremely difficult to resolve. Similarly, the average values of permeability obtained by modeling earthquake-hypocenter migration as a diffusive phenomenon (eqn 7) are smaller than the maximum values obtained when hypocenter migration is modeled as a solitary wave (cf. Miller *et al.* 2004).

In the absence of independent constraints, it is nonetheless reasonable to invoke crustal-scale permeability–depth relations (such as eqns 1, 2, 4, 12, and 13) to make first-order calculations related to large-scale hydraulic behavior (e.g. Fulton *et al.* 2009; Lyubetskaya & Ague 2009) or crustal-scale volatile and solute transport (e.g. Ingebritsen & Manning 2002). However, such permeability–depth relations likely reflect a dynamic competition between permeability creation and permeability destruction. Further, all such relations imply a porous-continuum model for permeability behavior that may be more aptly represented in terms of hydraulic seals (Miller *et al.* 2003; Audet *et al.* 2009), two-layer models (Hanano 1998), or multidimensional growth of multiple hydraulic fractures (Hill 1977; Sibson 1996; Miller & Nur 2000). The applicability of continuum modeling to represent (for instance) multiple fractures depends in large part on the size of model elements relative to fracture spacing. More realistic and better-constrained representation of permeability heterogeneity and anisotropy are essential to many practical applications.

ACKNOWLEDGEMENTS

We thank Shaul Hurwitz, Kurt Bucher, and an anonymous *Geofluids* referee for helpful reviews that greatly improved the final version of this paper.

REFERENCES

Ague JJ (1994) Mass transfer during Barrovian metamorphism of pelites, south-central Connecticut. II. Channelized fluid flow and the growth of staurolite and kyanite. *American Journal of Science*, **294**, 1,061–134.

Ague JJ (1997) Crustal mass transfer and index mineral growth in Barrow's garnet zone, northeast Scotland. *Geology*, **25**, 73–6.

Ague JJ, Baxter EF (2007) Brief thermal pulses during mountain building recorded by Sr diffusion in apatite and multicomponent diffusion in garnet. *Earth and Planetary Science Letters*, **261**, 500–16.

Audet P, Bostock MG, Christensen NI, Peacock SM (2009) Seismic evidence for overpressured subducted oceanic crust and megathrust fault sealing. *Nature*, **457**, 76–8.

Audin L, Avouac J-P, Flouzat M (2002) Fluid-driven seismicity in a stable tectonic context: the Remiremont fault zone, Vosges, France. *Geophysical Research Letters*, **29**; doi: 10.1029/2001GL012988.

Baker ET, Massoth GJ, Feely RA (1987) Cataclysmic hydrothermal venting on the Juan de Fuca Ridge. *Nature*, **329**, 149–51.

Baker ET, Lavelle JW, Feely RA, Massoth GJ, Walker SL, Lupton JE (1989) Episodic venting of hydrothermal fluids from the Juan de Fuca Ridge. *Journal of Geophysical Research*, **94**, 9,237–50.

Bickle MJ, McKenzie D (1987) The transport of heat and matter by fluids during metamorphism. *Contributions to Mineralogy and Petrology*, **95**, 644–65.

Brace WF (1980) Permeability of crystalline and argillaceous rocks. *International Journal of Rock Mechanics and Mining Sciences and Geomechanics Abstracts*, **17**, 241–51.

Cappa F, Rutqvist J, Yamamoto K (2009) Modeling crustal deformation and rupture processes related to upwelling of deep CO_2-rich fluids during the 1965-1967 Matsuhiro earthquake swarm in Japan. *Journal of Geophysical Research*, **114**; doi: 10.1029/2009JB006398.

Cathles LM, Adams JJ (2005) Fluid flow and petroleum and mineral resources in the upper (20 km) continental crust. *Economic Geology 100th Anniversary Volume*, 77–110.

Cathles LM, Erendi HJ, Barrie T (1997) How long can a hydrothermal system be sustained by a single intrusive event? *Economic Geology*, **92**, 766–71.

Challandes N, Marquer D, Villa IM (2008) P-T-t modelling, fluid circulation, and 39Ar-40Ar and Rb-Sr mica ages in the Aar Massif shear zones (Swiss Alps). *Swiss Journal of Geosciences*, **101**, 269–88.

Claesson L. (2007) *Fluid-rock interaction in two seismically active areas.* PhD thesis, Stockholm University, Sweden, 70 pp. + appendices.

Claesson L, Skelton A, Graham C, Morth CM (2007) The timescale and mechanisms of fault sealing and water-rock interaction after an earthquake. *Geofluids*, **7**, 427–40.

Clauser C (1992) Permeability of crystalline rocks. *Eos, Transactions American Geophysical Union*, **73**, 233.

Connolly JAD (1997) Devolatilization-generated fluid pressure and deformation-propagated fluid flow during prograde regional metamorphism. *Journal of Geophysical Research*, **102**, 18,149–73.

Cox SF (2002) Fluid flow in mid- to deep crustal shear systems: experimental constraints, observations on exhumed high fluid flux shear systems, and implications for seismogenic processes. *Earth Planets Space*, **4**, 1,121–5.

Cox SF, Knackstedt MA, Braun J (2001) Principles of structural control on permeability and fluid flow in hydrothermal systems. *Reviews in Economic Geology*, **14**, 1–24.

Dipple GM, Ferry JM (1992) Metasomatism and fluid flow in ductile fault zones. *Contributions to Mineralogy and Petrology*, **112**, 149–64.

Dutrow D, Norton D (1995) Evolution of fluid pressure and fracture propagation during contact metamorphism. *Journal of Metamorphic Geology*, **13**, 677–86.

Elkhoury JE, Brodsky EE, Agnew DC (2006) Seismic waves increase permeability. *Nature*, **441**, 1,135–8.

Elkhoury JE, Niemeijer A, Brodsky EE, Marone C (2010) Dynamic stress stimulates flow in fractures: laboratory observations of permeability enhancement. *Journal of Geophysical Research*, **115**; in press.

Evans KF, Genter A, Sausss J (2005) Permeability creation and damage due to massive fluid injections into granite at 3.5 km at Soultz: 1. Borehole observations. *Journal of Geophysical Research*, **110**; doi: 10.1029/2004JB003168.

Farver JR, Yund RA (1995) Grain boundary diffusion of oxygen, potassium and calcium in natural and hot-pressed feldspar aggregates. *Contributions to Mineralogy and Petrology*, **118**, 340–55.

Fischer T, Hainzl S, Eisner L, Shapiro SA, Le Calvez J (2008) Microseismic signatures of hydraulic fracture growth in sediment formations: observations and modeling. *Journal of Geophysical Research*, **113**; doi: 10.1029/2007JB005070.

Fornari DJ, Shank T, Von Damm KL, Gregg TKP, Lilley M, Levai G, Bray A, Haymon RM, Perfit MR, Lutz R (1998) Time-series temperature measurements at high-temperature hydrothermal vents, East Pacific Rise 9°49′–51′N: evidence for monitoring a crustal cracking event. *Earth and Planetary Science Letters*, **160**, 419–31.

Fulton PM, Saffer DM, Bekins BA (2009) A critical evaluation of crustal dehydration as the cause of an overpressured and weak San Andreas Fault. *Earth and Planetary Science Letters*, **284**, 447–54.

Fyfe WS, Price NJ, Thompson AB (1978) *Fluids in the Earth's Crust.* Elsevier Scientific, New York.

Germanovich LN, Lowell RP (1992) Percolation theory, thermoelasticity, and discrete hydrothermal venting in the Earth's crust. *Science*, **255**, 1564–7.

Gillis KM, Roberts MD (1999) Cracking at the magma-hydrothermal transition: evidence from the Troodos Ophiolite, Cyprus. *Earth and Planetary Science Letters*, **169**, 227–44.

Golden CE, Webb SC, Sohn RA (2003) Hydrothermal microearthquake swarms beneath active vents at Middle Valley, northern Juan de Fuca Ridge. *Journal of Geophysical Research*, **108**; doi: 10.1029/2001JB000226.

Hanano M (1998) A simple model of a two-layered high-temperature liquid-dominated geothermal reservoir as part of a large-scale hydrothermal convection system. *Transport in Porous Media*, **33**, 3–27.

Hanson RB (1992) Effects of fluid production on fluid flow during regional and contact metamorphism. *Journal of Metamorphic Geology*, **10**, 87–97.

Hanson RB (1995) The hydrodynamics of contact metamorphism. *Geological Society of America Bulletin*, **107**, 595–611.

Hanson RB (1997) Hydrodynamics of regional metamorphism due to continental collision. *Economic Geology*, **92**, 880–91.

Häring MO, Schanz U, Ladner F, Dyer BC (2008) Characterisation of the Basel 1 enhanced geothermal system. *Geothermics*, **37**, 469–95.

Haymon RM (1996) The response of ridge-crest hydrothermal systems to segmented, episodic magma supply. *Geological Society Special Publication*, **118**, 157–68.

Hill DP (1977) A model for earthquake swarms. *Journal of Geophysical Research*, **82**, 347–52.

Hill DP, Reasenberg PA, Michael A, Arabaz WJ, Beroza G, Brumbaugh D, Brune JN, Castro R, Davis S, dePolo D, Ellsworth WL, Gomberg J, Harmsen S, House L, Jackson SM, Johnston MJS, Jones L, Keller R, Malone S, Munguia L, Nava S, Pechmann JC, Sanford A, Simpson RW, Smith RB, Stark M, Stickney M, Vidal A, Walter S, Wong V, Zollweg J (1993) Seismicity remotely triggered by the magnitude 7.3 Landers, California, earthquake. *Science*, **260**, 1,617–23.

Hill DP, Prejean S (2005) Magmatic unrest beneath Mammoth Mountain, California. *Journal of Volcanology and Geothermal Research*, **146**, 257–83.

Horalek J, Fischer T (2008) Role of crustal fluids in triggering the West Bohemia/Vogtland earthquake swarms: just what we know (a review). *Studies in Geophysics and Geodesy*, **52**, 455–78.

Hsieh PA (1998) Scale effects in fluid flow through fractured geologic media. In: *Scale Dependence and Scale Invariance in Hydrology* (ed. Sposito G), pp. 335–53. Cambridge University Press, New York.

Hsieh PA, Bredehoeft JD (1981) A reservoir analysis of the Denver earthquakes: a case of induced seismicity. *Journal of Geophysical Research*, **86**, 903–20.

Husen S, Taylor R, Smith RB, Heasler H (2004) Changes in geyser eruption behavior and remotely triggered seismicity in Yellowstone National Park produced by the 2002 M 7.9 Denali fault earthquake, Alaska. *Geology*, **32**, 537–40.

Ingebritsen SE, Manning CE (1999) Geological implications of a permeability-depth curve for the continental crust. *Geology*, **27**, 1,107–10.

Ingebritsen SE, Manning CE (2002) Diffuse fluid flux through orogenic belts: implications for the world ocean. *Proceedings of the National Academy of Sciences, USA*, **99**, 9,113–6.

Ingebritsen SE, Scholl MA (1993) The hydrogeology of Kilauea volcano. *Geothermics*, **22**, 255–70.

Johnson HP, Hutnak M, Dziak RP, Fox CG, Urcuyo I, Cowen JP, Nabelek J, Fisher C (2000) Earthquake-induced changes in a hydrothermal system on the Juan de Fuca mid-ocean ridge. *Nature*, **407**, 174–7.

Kitagawa Y, Fujimori K, Koizumi N (2007) Temporal change in permeability of the Nojima Fault zone by repeated water injection experiments. *Tectonophysics*, **443**, 183–92.

Lancaster PJ, Baxter EF, Ague JJ, Breeding CM, Owens TL (2008) Synchronous peak Barrovian metamorphism driven by syn-orogenic magmatism and fluid flow in southern Connecticut, USA. *Journal of Metamorphic Geology*, **26**, 527–38.

Lowell RP, Van Cappellen P, Germanovich LN (1993) Silica precipitation in fractures and the evolution of permeability in hydrothermal upflow zones. *Science*, **260**, 192–4.

Lyubetskaya T, Ague JJ (2009) Modeling the magnitudes and directions of regional metamorphic fluid flow in collisional orogens. *Journal of Petrology*, **50**, 1,505–31.

Manga M (1996) Hydrology of spring-dominated streams in the Oregon Cascades. *Water Resources Research*, **32**, 2,435–9.

Manga M (1997) A model for discharge in spring-dominated streams and implications for the transmissivity and recharge of Quaternary volcanics in the Oregon Cascades. *Water Resources Research*, **33**, 1,813–22.

Manga M, Rowland JC (2009) Response of Alum Rock springs to the October 30, 2007 Alum Rock earthquake and implications for the origin of increased discharge after earthquakes. *Geofluids*, **9**, 237–50.

Manning CE, Bird DK (1991) Porosity evolution and fluid flow in the basalts of the Skaergaard magmatic-hydrothermal system, East Greenland. *American Journal of Science*, **291**, 201–57.

Manning CE, Ingebritsen SE (1999) Permeability of the continental crust: the implications of geothermal data and metamorphic systems. *Reviews of Geophysics*, **37**, 127–50.

Manning CE, Ingebritsen SE, Bird DK (1993) Missing mineral zones in contact metamorphosed basalts. *American Journal of Science*, **293**, 894–938.

Miller SA, Nur A (2000) Permeability as a toggle switch in fluid-controlled crustal processes. *Earth and Planetary Science Letters*, **183**, 133–46.

Miller SA, van der Zee W, Olgaard DL, Connolly JAD (2003) A fluid pressure-feedback model of dehydration reactions: experiments, modelling, and application to subduction zones. *Tectonophysics*, **370**, 241–51.

Miller SA, Collettini C, Chiaraluce L, Cocco M, Barchi M, Kaus BJP (2004) Aftershocks driven by a high-pressure CO_2 source at depth. *Nature*, **427**, 724–7.

Mitchell JK (1993) *Fundamentals of Soil Behavior*, 2nd edn. John Wiley and Sons, New York.

Moore DE, Morrow CA, Byerlee JD (1983) Chemical reactions accompanying fluid flow through granite held in a temperature gradient. *Geochimica et Cosmochimica Acta*, **47**, 445–53.

Moore DE, Lockner DA, Byerlee JD (1994) Reduction of permeability in granite at elevated temperatures. *Science*, **265**, 1,558–61.

Morrow C, Lockner D, Moore D, Byerlee J (1981) Permeability of granite in a temperature gradient. *Journal of Geophysical Research*, **86**, 3,002–8.

Morrow CA, Moore DE, Lockner DA (2001) Permeability reduction in granite under hydrothermal conditions. *Journal of Geophysical Research*, **106**, 30,551–60.

Neuzil CE (1995) Abnormal pressures as hydrodynamic phenomena. *American Journal of Science*, **295**, 742–86.

Nippress SEJ, Rietbrock A (2007) Seismogenic zone high permeability in the central Andes inferred from relocations of microearthquakes. *Earth and Planetary Science Letters*, **263**, 235–45.

Noir J, Jacques E, Bekri S, Adler PM, Tapponnier P, King GCP (1997) Fluid flow triggered migration of events in the 1989 Dobi earthquake sequence of Central Afar. *Geophysical Research Letters*, **24**, 2,335–8.

Ohtake M (1974) Seismic activity induced by water injection at Matsuhiro, Japan. *Journal of Physics of the Earth*, **22**, 163–76.

Polak A, Elsworth D, Yasuhara H, Grader AS, Halleck PM (2003) Permeability reduction of a natural fracture under net dissolution by hydrothermal fluids. *Geophysical Research Letters*, **30**; doi: 10.1029/2003GL017575.

Rojstaczer SA, Wolf S. (1994). Hydrologic changes associated with the earthquake in the San Lorenzo and Pescadero drainage basins. In: *The Loma Prieta, California Earthquake of October 17, 1989 – Hydrologic Disturbances* (ed. Rojstaczer SA), *US Geological Survey Professional Paper* **1551-E**, E51–64.

Rojstaczer SA, Wolf S, Michel R (1995) Permeability enhancement in the shallow crust as a cause of earthquake-induced hydrological changes. *Nature*, **373**, 237–9.

Rojstaczer SA, Ingebritsen SE, Hayba DO (2008) Permeability of continental crust influenced by internal and external forcing. *Geofluids*, **8**, 128–39.

Saar MO, Manga M (2004) Depth dependence of permeability in the Oregon Cascades inferred from hydrogeologic, thermal, seismic, and magmatic modeling constraints. *Journal of Geophysical Research*, **109**; doi: 10.1029/2003JB002855.

Sato T, Sakai R, Furuya K, Kodama T (2000) Coseismic spring flow changes associated with the 1995 Kobe earthquake. *Geophysical Research Letters*, **27**, 1,219–22.

Shapiro SA, Dinske C (2009) Fluid-induced seismicity: pressure diffusion and hydraulic fracturing. *Geophysical Prospecting*, **57**, 301–10.

Shapiro SA, Huenges E, Borm G (1997) Estimating the crust permeability from fluid-injection induced seismic emission at the KTB site. *Geophysical Journal International*, **131**, F15–8.

Shmonov VM, Vitiovtova VM, Zharikov AV, Grafchikov AA (2002) Fluid permeability of the continental crust: estimation from experimental data. *Geochemistry International*, **40**(Suppl. 1), S3–13.

Shmonov VM, Vitiovtova VM, Zharikov AV, Grafchikov AA (2003) Permeability of the continental crust: implications of experimental data. *Journal of Geochemical Exploration*, **78–79**, 697–9.

Sibson RH (1996) Structural permeability of fluid-driven fault-fracture meshes. *Journal of Structural Geology*, **18**, 1031–42.

Sibson RH, Rowland JV (2003) Stress, fluid pressure, and structural permeability in seismogenic crust, North Island, New Zealand. *Geophysical Journal International*, **154**, 584–94.

Sibson RH, Moore JMM, Rankin AH (1975) Seismic pumping – a hydrothermal fluid transport mechanism. *Journal of the Geological Society of London*, **131**, 653–9.

Sohn RA (2007) Stochastic analysis of exit fluid temperature records from the active TAG hydrothermal mound (Mid-Atlantic Ridge, 26°N): 1. Modes of variability and implications for subsurface flow. *Journal of Geophysical Research*, **112**; doi: 10.1029/2006JB004435.

Sohn RA, Fornari DJ, Von Damm KL, Hildebrand JA, Webb SC (1998) Seismic and hydrothermal evidence for a cracking event on the East Pacific rise crest at 9°50′ N. *Nature*, **396**, 159–61.

Stein JS, Fisher AT (2003) Observations and models of lateral hydrothermal circulation on young ridge flank: numerical evaluation of thermal and chemical constraints. *Geochemistry Geophysics Geosystems*, **4**; doi: 10.1029/2002GC000415.

Stober I, Bucher K (2007) Hydraulic properties of the crystalline basement. *Hydrogeology Journal*, **15**, 213–24.

Summers R, Winkler K, Byerlee J (1978) Permeability changes during the flow of water through Westerly Granite at temperatures of 100°–400°C. *Journal of Geophysical Research*, **83**, 339–44.

Talwani P, Acree S (1984) Pore pressure diffusion and the mechanism of reservoir induced seismicity. *Pure and Applied Geophysics*, **122**, 947–65.

Talwani P, Chen L, Gahalaut K (2007) Seismogenic permeability, k_s. *Journal of Geophysical Research*, **112**; doi: 10.1029/2006JB004665.

Tanaka H, Chester FM, Mori JJ, Wang C-Y (2007) Preface – drilling into fault zones. *Tectonophysics*, **44**, 123–5.

Tenthorey E, Scholz CH, Aharonov E, Leger A (1998) Precipitation sealing and diagenesis 1. Experimental results. *Journal of Geophysical Research*, **103**, 23,951–67.

Titley SR (1990) Evolution and style of fracture permeability in intrusion-centered hydrothermal systems. In: *The Role of Fluids in Crustal Processes* (eds Bredehoeft JD, Norton DL), pp. 50–63. National Academy Press, Washington, DC.

Townend J, Zoback MD (2000) How faulting keeps the crust strong. *Geology*, **28**, 399–402.

Urabe T, *et al.* (1995) The effect of magmatic activity on hydrothermal venting along the superfast-spreading East Pacific Rise. *Science*, **269**, 1,092–5.

Vaughan PJ, Moore DE, Morrow CA, Byerlee JD (1986) Role of cracks in progressive permeability reduction during flow of heated aqueous fluids through granite. *Journal of Geophysical Research*, **91**, 7,517–30.

Waite GP, Smith RB (2002) Seismic evidence for fluid migration accompanying subsidence of the Yellowstone caldera. *Journal of Geophysical Research*, **107**, doi:10.1029/2001JB000586.

Walder J, Nur A (1984) Porosity reduction and crustal pore pressure development. *Journal of Geophysical Research*, **89**, 11,539–48.

Winograd IJ (1971) Hydrogeology of ash-flow tuff: a preliminary statement. *Water Resources Research*, **7**, 994–1006.

Yardley BWD (1986). Fluid migration and veining in the Connemara Schists. In: *Fluid-Rock Reactions During Metamorphism, Advances in Physical Geochemistry* **5** (eds Walther JV, Wood BJ), pp. 109–31. Springer-Verlag, New York.

Yardley BWD, Baumgartner LP (2007). Fluid processes in deep crustal fault zones. In: *Tectonic Faults – Agents of Change on a Dynamic Earth* (eds Handy MR, Hirth G, Hovius N), pp. 295–318. The MIT Press, Cambridge.

Yardley BWD, Valley JW (1997) The petrologic case for a dry lower crust. *Journal of Geophysical Research*, **102**, 12,173–85.

Yasuhara H, Polak A, Mitani Y, Grader AS, Halleck PM, Elsworth D (2006) Evolution of fracture permeability through fluid-rock reaction under hydrothermal conditions. *Earth and Planetary Science Letters*, **244**, 186–200.

Zhang S, Paterson MS, Cox SF (2001) Microcrack growth and healing in deformed calcite aggregates. *Tectonophysics*, **335**, 17–36.